

Article

Assessing the Impacts of Extreme Climate Events on Vegetation Activity in the North South Transect of Eastern China (NSTEC)

Yi Zhou ¹, Fengsong Pei ^{1,*}, Yan Xia ¹, Changjiang Wu ², Rui Zhong ¹, Kun Wang ¹, Huaili Wang ¹ and Yang Cao ¹

¹ School of Geography, Geomatics and Planning, Jiangsu Normal University, No. 101 Shanghai Road, Tongshan New District, Xuzhou 221116, China; yzhou@jsnu.edu.cn (Y.Z.); xiayan@jsnu.edu.cn (Y.X.); zhongrui09@foxmail.com (R.Z.); 18361299171kun@gmail.com (K.W.); wanghl@jsnu.edu.cn (H.W.); 3020174308@jsnu.edu.cn (Y.C.)

² School of Geography and Planning, Sun Yat-sen University, Guangzhou 510275, China; wuchj9@mail2.sysu.edu.cn

* Correspondence: peifs@jsnu.edu.cn; Tel.: +86-516-8340-3865

Received: 11 September 2019; Accepted: 31 October 2019; Published: 1 November 2019



Abstract: Extreme climate events frequently exert serious effects on terrestrial vegetation activity. However, these effects are still uncertain in widely distributed areas with different climate zones. Transect analysis is important to understand how terrestrial vegetation responds to climate change, especially extreme climate events, by substituting space for time. In this paper, seven extreme climate indices and the Normalized Difference Vegetation Index (NDVI) are employed to examine changes in the extreme climate events and vegetation activity. To reduce the uncertainty of the NDVI, two satellite-derived NDVI datasets, including the third generation Global Inventory Monitoring and Modeling System (GIMMS-3g) NDVI dataset and the NDVI from the National Oceanic and Atmospheric Administration (NOAA) satellites on Star Web Servers (SWS), were employed to capture changes in vegetation activity. The impacts of climate extremes on vegetation activity were then assessed over the period of 1982–2012 using the North–South Transect of Eastern China (NSTEC) as a case. The results show that vegetation activity was overall strengthened from 1982 to 2012 in the NSTEC. In addition, extreme high temperature events revealed an increased trend of approximately 5.15 days per decade, while a weakened trend (not significant) was found in extreme cold temperature events. The strengthened vegetation activities could be associated with enhanced extreme high temperature events and weakened extreme cold temperature events over the past decades in most of the NSTEC. Despite this, inversed changes were also found locally between vegetation activity and extreme climate events (e.g., in the Northeast Plain). These phenomena could be associated with differences in vegetation type, human activity, as well as the combined effects of the frequency and intensity of extreme climate events. This study highlights the importance of accounting for the vital roles of extreme climate effects on vegetation activity.

Keywords: vegetation activity; extreme climate events; Normalized Difference Vegetation Index; North-South Transect of Eastern China

1. Introduction

Past studies showed that the global mean temperature rose by approximately 0.85 °C from 1880 to 2012 [1,2]. However, changes in extreme climate events are more uncertain than average climate conditions. With increasing global climate warming, extreme climate events, including temperature extremes and precipitation extremes, occur more frequently than ever before. This phenomenon exerts

serious effects on humans due to probable flooding, droughts, and so on [3–6], and has become a research focus for the scientific community.

The NDVI (Normalized Difference Vegetation Index) provides a critical historical perspective on vegetation activities. The consistency of the NDVI derived from various sensors in satellites has been evaluated with ground-based sensors [7,8]. On these bases, the NDVI is widely employed to detect vegetation dynamics, as well as responses to climate change at regional and global scales [9–15]. Climate extremes could alter physiological and ecological processes and even ecosystem functions in the terrestrial ecosystem [16,17]. For instance, Barichivich et al. analyzed the relationships between multiple climate and vegetation indicators of the growing season of northern ecosystems and their connection with the carbon cycle using NDVI as the indicator [14]. Tan et al. explored the relationships between vegetation growth and climate extremes in the Poyang Lake River Basin [18]. They found that variations in the NDVI are generally determined by temperature but not precipitation extremes. Sangeeta et al. studied the characterization of vegetation dynamics over South Asia using satellite time series of different NDVI sources and found that the spatiotemporal vegetation trends derived from the NDVI-3g are analogous to both the NDVI and EVI from the Moderate-Resolution Imaging Spectroradiometer (MODIS) for the Earth Observing System (EOS), thereby indicating greening over semi-arid regions [19]. Zhao et al. studied the change of vegetation growth and its correlation with extreme climate events in the Loess Plateau. They found that vegetation coverage responded positively to precipitation and temperature extremes in the region [20]. By using Xinjiang in China as a case study, Yao et al. showed that climate extremes could have negative effects on vegetation growth in the arid region of Central Asia [21]. Li et al. estimated the trends of several extreme climate indices and the NDVI in the Mongolia Plateau. They found positive correlations between most of the extreme climate indices and the NDVI at monthly and seasonal scales [22]. Despite being widely employed in past studies, remote sensed data are affected by several disturbances when monitoring vegetation activities, including systematic errors, accidental errors, and problematic processing methods [23,24]. In addition, past studies were frequently performed by taking topographic units such as plateaus or basins as the case. Instead, transect analysis is an important and effective approach to understand how terrestrial ecosystems would respond to global climate change by substituting space for time [25,26].

By using the North–South Transect of Eastern China (NSTEC) as a case, this paper analyzes the impacts of climate extremes (i.e., temperature extremes and precipitation extremes) on terrestrial vegetation activity over the period of 1982–2012. The NSTEC is one of the 15 global climate change transections in the International Geosphere–Biosphere Programme (IGBP) [25]. It encompasses a large climate gradient spanning from temperate to tropical climates. Specifically, this paper aims to (1) examine the spatiotemporal variation of vegetation activity in the NSTEC using two different satellite-derived NDVI datasets; (2) analyze the changes in extreme climate events using seven extreme climate indices from the Expert Team on Climate Change Detection and Indices (ETCCDI); (3) explore the relationships between vegetation activity and extreme climate events.

2. Study Area and Data Preprocessing

2.1. Study Area

The North–South Transect of Eastern China (NSTEC), which covers about 2.88 million km², is located within 108°–118° E, 18°10′–40° N and 118°–128° E, 40°–53°33′ N. The NSTEC lies across different climate zones from tropical climates to cold temperate climates. Thus, the temperature in the NSTEC ranges from 38.9 °C to −44.6 °C, and the annual total precipitation decreases from 2000 mm in the southernmost part of Hainan to about 600 mm in the northern Heilongjiang Province (Figure 1). Meanwhile, the NSTEC is well known for its diversified landscapes, including Great Hinggan Mountains (G1), Inner Mongolia Plateau (G2), Northeast Plain (G3), Changbai Mountain (G4), Loess Plateau (G5), North China Plain (G6), Jiangnan-Dongting-Lake Plain (G7), Yangtze River

Basin (G8), Wuyishan District (G9), and Pearl River Delta (G10) in Figure 1. Terrestrial vegetation mainly includes cultivated vegetation, coniferous forests, broad-leaved forests, shrubs, and grasslands.

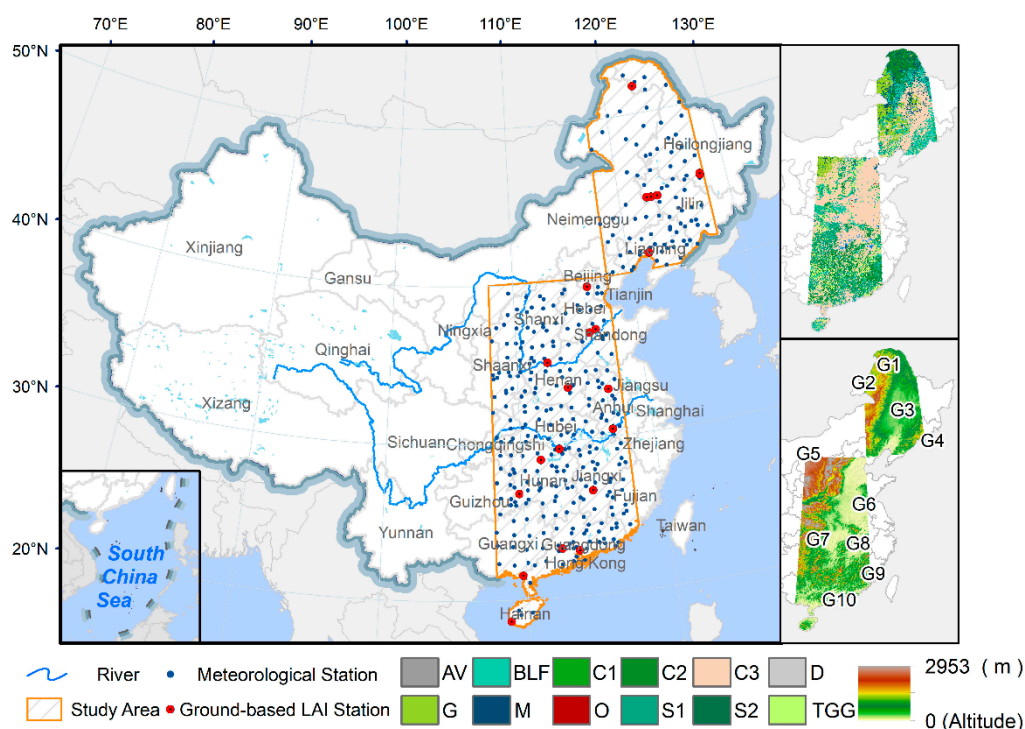


Figure 1. The distribution of meteorological stations, ground-based LAI stations, vegetation types, and geomorphological types in the NSTEC. (Vegetation type, BLF: Broad-Leaved Forest, C1: Coniferous Broad-Leaved Mixed Forest, C2: Coniferous Forest, C3: Cultivated Vegetation, G: Grassland, M: Meadow, O: Other Type, S1: Shrub, TGG: Thick Growth of Grass. Geomorphic type, G1: Great Hinggan Mountains, G2: Inner Mongolia Plateau, G3: Northeast Plain, G4: Changbai Mountain, G5: Loess Plateau, G6: North China Plain, G7: Jiangnan-Dongting-Lake Plain, G8: Yangtze River Basin, G9: Wuyishan District, and G10: Pearl River Delta).

2.2. Data and Preprocessing

The data sources in this study include satellite-based NDVI data, Leaf Area Index (LAI) data, daily meteorological data, and some other auxiliary data (e.g., climate zones, vegetation types, and elevation data). In detail, weekly NDVI data, which cover the period of 1982–2012, were obtained from National Oceanic and Atmospheric Administration (NOAA) satellites on Star Web Servers (NOAA-SWS) at a resolution of 4 km. In addition, the GIMMS-3g NDVI dataset, at a resolution of 8 km, was obtained from the third generation Global Inventory Monitoring and Modeling System (GIMMS) from the Advanced Very High Resolution Radiometer (AVHRR) sensors. The dataset has been corrected for sensor degradation, inter-sensor differences, cloud cover, solar zenith angle, viewing angle effects due to satellite drift, and volcanic aerosols [27]. The NDVI data were then synthesized to monthly and yearly scales, respectively. In addition, the annual maximum LAI data were obtained from the long-term ground-based observations of China FLUX and published studies [28] (Figure 1).

For the meteorological data, the daily maximum temperature, daily minimum temperature, and daily precipitation data were collected over the period of 1982–2012 from the National Meteorological Information Center in China. Quality control of the data was first conducted via a manual inspection of time consistency and extremum validation [29]. We further validated the data by screening and eliminating suspicious and missing records to ensure their continuity and consistency. In detail, the stations that were newly-built or abandoned later were removed to ensure the data's consistency and accuracy. Finally, 355 meteorological stations were selected for further analysis. To extract the

corresponding NDVI value around the meteorological stations, the grid value of the site's location was extracted to participate in subsequent calculations using the Geographic Information System (GIS).

3. Methods

3.1. Monitoring Vegetation Activities by Using the NDVI as an Indicator

At present, more than 30 vegetation indices, including the NDVI, the Enhanced Vegetation Index (EVI), and the Difference Vegetation Index (DVI), were developed to reflect changes in vegetation activities [30–33]. Although many new vegetation indices were proposed to account for many factors, such as soil and atmospheric effects [11], the NDVI is still a good indicator when dealing with large-scale vegetation coverage and vegetation productivity [34–36]. For instance, Barichivich et al. found that the GIMMS-3g is highly consistent with MODIS NDVI [14]. In this paper, the NDVI was employed as an indicator to monitor changes in vegetation activities in the NSTEC. To reduce the uncertainty of the NDVI datasets at different resolutions, two satellite-based NDVI datasets from GIMMS-3g and NOAA-SWS were employed due to the dramatic improvement of the GIMMS-3g and NOAA-SWS datasets [37–39]. In detail, monthly and yearly NDVIs were synthesized from the original weekly data. A simple linear regression was then conducted to examine the linear trend of the NDVI (Y) [40,41]

$$Y = at + b \quad (1)$$

where t is the time period(year), and a and b are regression coefficients. If a is larger (or less) than zero at a 95% significance level, then there is statistical evidence to support the presence of increased (or decreased) trends of the NDVI (i.e., vegetation activity). In this paper, linear regression was performed using the R Software [42] and the trend package [43].

3.2. Characterizing Extreme Climate Events Using Extreme Climate Indices

The climate extreme index (CEI) was first proposed in the United States in 1996. However, the CEI was found to have some limitations, such as its lack of suitability and effectiveness when applied to other countries and regions [44]. The European Climate Assessment (ECA) indices were then developed by accounting for temperature, precipitation, frost, and growth season [45]. Many climate extreme indices, including most of the ECA indices, were also proposed by the Expert Team on Climate Change Detection and Indices (ETCCDI) [46]. The ETCCDI has been used in the fourth and fifth Intergovernmental Panel on Climate Change (IPCC) [47,48], which makes the indices widely used in extreme climate events [49–51].

In this paper, seven indices from the ETCCDI were selected to reflect the intensity and frequency of extreme climate events to examine the changes in temperature and precipitation extremes in the NSTEC (Table 1). In detail, this study includes three extreme cold temperature indices (CSDI, TNN, and TN10p), three extreme high temperature indices (WSDI, TXX, and TX90p), and one extreme precipitation index (R95p). TXX and TNN reflect the intensity of extreme temperature events. In addition, the R95p is employed to characterize the extreme precipitation intensity. The remaining four indices, TN10p, TX90p, CSDI, and WSDI, represent the frequency of extreme temperature events.

Table 1. Extreme climate indices in this paper.

Name	Definitions	Units
TN10p	Percentage of time when daily min temperature <10th percentile	days
TX90p	Percentage of time when daily max temperature >90th percentile	days
TXX	Monthly maximum value of daily max temperature	°C
TNN	Monthly minimum value of daily min temperature	°C
WSDI	Annual count when at least six consecutive days of max temperature >90th percentile	days
CSDI	Annual count when at least six consecutive days of min temperature <10th percentile	days
R95p	Annual total precipitation from days >95th percentile	mm

To examine changes in the intensity of extreme climate events, linear regression was also performed using TXX, TNN, and R95p as indicators. If the slope (a in Equation (1)) is larger (or smaller) than zero, there is an increased (or decreased) trend in the extreme climate events.

Given the discrete nature of the frequency of extreme climate events, a Poisson regression model was employed to examine their monotonic trends. If the probability of a random variable N equals k , then we get the Poisson distribution density function as Equation (2).

$$p(N_i = k|\lambda_i) = \frac{e^{-\lambda_i} \lambda_i^k}{k!} (k = 0, 1, 2 \dots) \quad (2)$$

where k represents the frequency of the observed samples at a certain time, and λ_i is the parameter of incidence. To evaluate whether the extreme precipitation frequency at each station has an increasing or decreasing statistical trend, a linear relationship between occurrence rate parameters (λ) and time (t) is established:

$$\lambda_i = e^{\beta_0 + \beta_1 \cdot t_i} \quad (3)$$

If the regression coefficient β is larger (or smaller) than zero at 5%, statistical evidence is found to support temporal trends in the occurrence of extreme climate events. In this paper, Poisson regression was applied in four indices, including TN10p, TX90p, CSDI, and WSDI, respectively. Similarly, all these algorithms were performed using the R Software [42] and the trend package [43].

3.3. Assessing the Impacts of Extreme Climate Events on Vegetation Activities

The LAI, which is defined as one half of the total green leaf area per unit ground surface area [52], has been widely used to characterize the structure and function of vegetation [53]. In this paper, the LAI data from ground observation were used to verify the reliability of the aforementioned two NDVI datasets. On this basis, we examined the spatiotemporal trends of the vegetation activity over the period 1982–2012 in the NSTEC using the NDVI as an indicator. The changes in climate extremes, including extreme temperature events and extreme precipitation events, were analyzed using the aforementioned seven extreme climate indices from ETCCDI as indicators. Pearson correlation analyses were then conducted between extreme climate indices, and the corresponding NDVI values were sampled according to the meteorological stations. The combined effects of the frequency and intensity of extreme climate events on vegetation activities were also analyzed based on these numerical values. The effect of extreme climate events on vegetation activity was further analyzed by climatic ecozones in the NSTEC. Possible causes of vegetation activity changes to extreme climate events were then discussed from the aspects of vegetation type, human activity, and the combined effects of the frequency and intensity of extreme climate events.

4. Results and Discussions

4.1. Validation of the NDVI Datasets

In past studies, many NDVI datasets were widely evaluated through sample-based validation or comparison with existing NDVI products by third-party researchers. For instance, Fensholt and Proud [54] compared the performances of a time series of GIMMS and MODIS NDVI data to evaluate long-term vegetation trends at a global scale. In this paper, the accuracy of the aforementioned NDVI datasets was further evaluated by comparing it to ground-based LAI observations. As seen in Figure 2, a significant correlation was found between the NOAA-SWS-derived NDVI and the LAI ($R = 0.768$, $N = 22$, $P = 0.000$). Similarly, a significant correlation was also found between the GIMMS-3g-derived NDVI ($R = 0.769$, $N = 22$, $P = 0.000$) and the ground-based LAI.

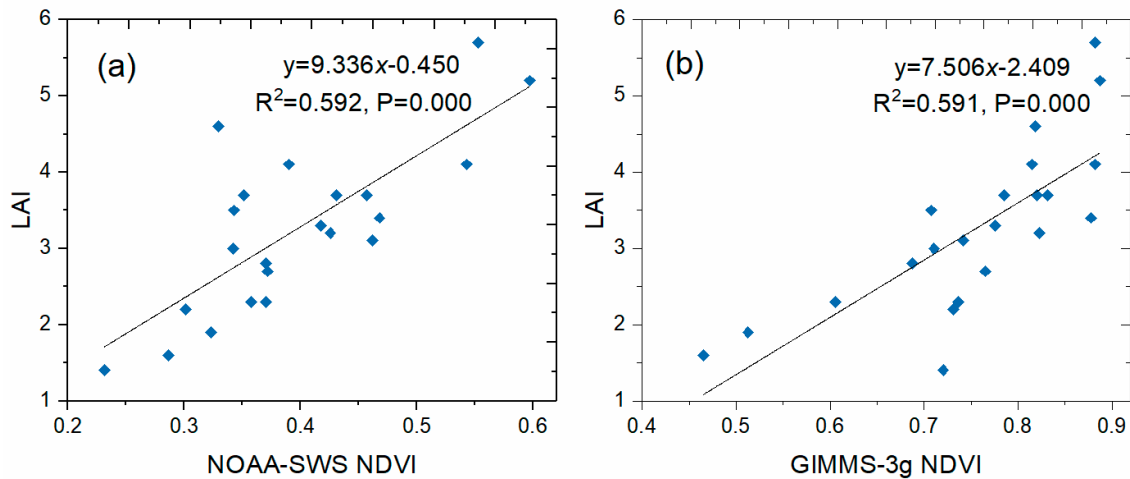


Figure 2. Relationships between LAI and the (a) NOAA-SWS NDVI, (b) GIMMS-3g NDVI.

4.2. Spatiotemporal Variations of Vegetation Activity and Extreme Climate Events in the NSTEC

4.2.1. Variations of Vegetation Activity

As shown in Figure 3, the two NDVI datasets linearly fit close to each other. Specifically, both the satellite-derived observations from the GIMMS-3g and NOAA-SWS NDVI datasets revealed increasing trends from 1982 to 2012 at a rate of 0.0113 ± 0.0026 per decade ($R^2 = 0.386$) from the SWS and 0.0111 ± 0.0026 per decade ($R^2 = 0.526$) from the GIMMS-3g, respectively. These results indicate the overall enhanced vegetation activity in the past few decades (taking the NSTEC as a whole).

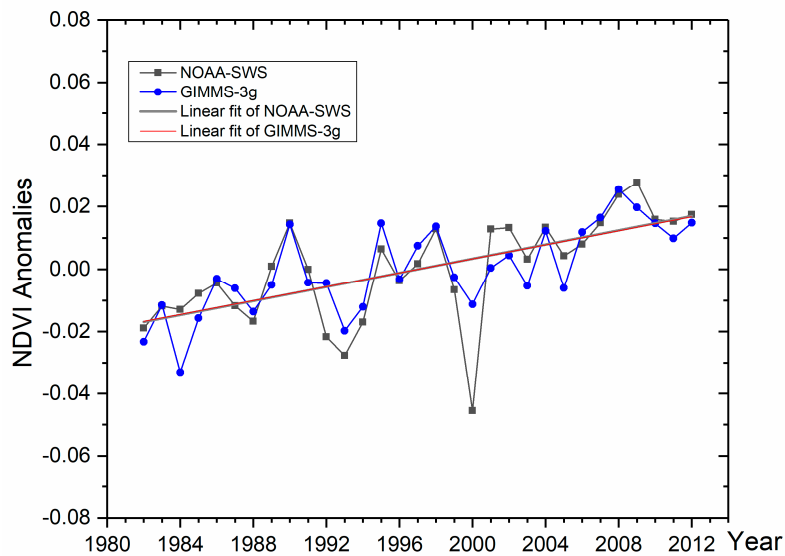


Figure 3. Interannual variations in anomalies of mean NDVI from 1982 to 2012 (the linear fit of the two NDVI datasets are close).

The spatial heterogeneity in the vegetation activity was further analyzed by examining the annual mean values and trends of the NDVI from 1982 to 2012. We found that the mean NDVI is relatively high in broad-leaved forests and coniferous forests in the regions including the Greater Khingan Range (G1) and the Changbai Mountains (G4) in the northeastern NSTEC, the Qinling Mountains in the Central parts of the NSTEC, the Wuyi Mountains (G9), and the Hainan Island in the southern NSTEC. On the contrary, the lowest NDVI was found in grasslands and human land-use areas. Concretely, the areas with relatively small NDVIs were mainly distributed in the Northeast Plain (G3), the Loess Plateau (G5), the Yangtze River Basin (G8), and the Pearl River Delta (G10).

Figure 4 shows the spatial patterns of the trend in NDVI derived from the GIMMS-3g and NOAA-SWS datasets during the period from 1982 to 2012. Both datasets revealed ascending trends in most parts of the NSTEC over the past decades. Nevertheless, decreased NDVI could also be found in the Inner Mongolia Plateau (G2), the eastern Great Hinggan Mountains (G1), and the Pearl River Basin (G10) in Figures 1 and 4. The NDVI trend was further analyzed by vegetation types. The results showed that all types of vegetation had mainly increased trends in the NSTEC over the past few decades. Specifically, 73% of tropical rainforests showed an increasing trend, reaching 0.00185-year^{-1} in Hainan Island. The slowest growth was found in temperate coniferous and broad-leaved mixed forests at approximately 0.0084 per decade.

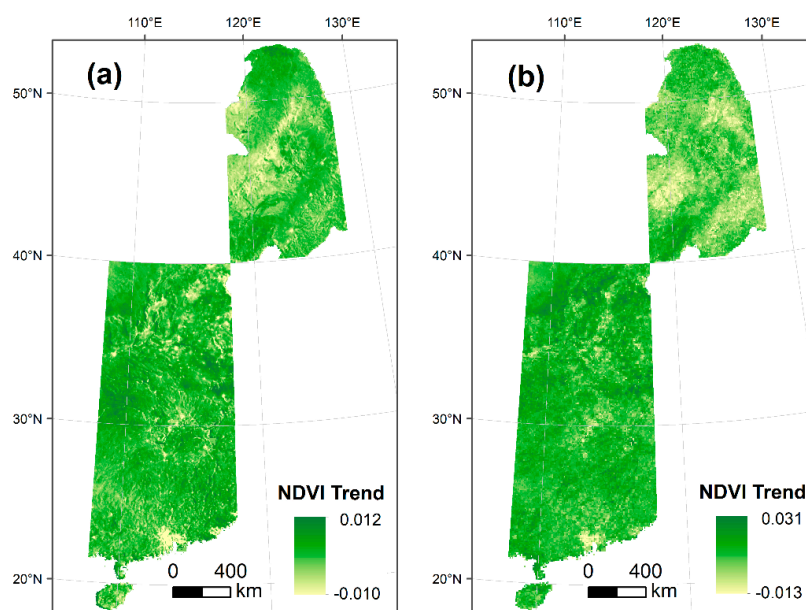


Figure 4. Trend of NDVI from 1982 to 2012 in the NSTEC: (a) NOAA-SWS; (b) GIMMS-3g.

4.2.2. Frequency of Extreme Temperature Events

As shown in Figure 5, extreme cold temperature indices, including CSDI and TN10p, revealed decreased trends at a rate of $-0.066 \pm 0.112\text{ days}\cdot\text{year}^{-1}$ ($R^2 = 0.012$, $P = 0.230$) and $-0.230 \pm 0.166\text{ days}\cdot\text{year}^{-1}$ ($R^2 = 0.062$, $P = 0.177$). On the contrary, extreme high temperature indices showed obvious upward trends, reaching $0.136 \pm 0.041\text{ days}\cdot\text{year}^{-1}$ for the WSDI ($R^2 = 0.278$, $P = 0.002$) and $0.515 \pm 0.088\text{ days}\cdot\text{year}^{-1}$ for the TX90p ($R^2 = 0.544$, $P = 0.000$).

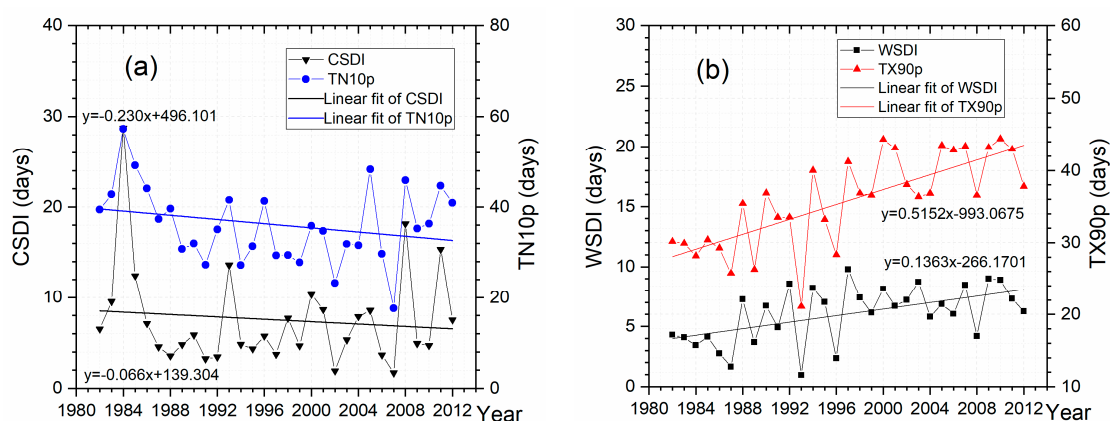


Figure 5. The temporal variations of extreme climate indices from 1982 to 2012: (a) CSDI and TN10p; (b) WSDI and TX90p.

We first analyzed the spatial patterns of the mean annual precipitation from 1982 to 2012 in the NSTEC (Figure 6a). We found that it decreased from southeast to northwest, owing to the combining influences of southeast monsoons and southwest monsoons [55]. Furthermore, we analyzed the spatial heterogeneity of the trends in extreme temperature frequencies using CSDI, TN10p, WSDI, and TX90p as indicators (Figure 6b–e). For extreme cold temperature events, an overall decreasing trend could be found in the NSTEC based on an analysis of the two extreme cold temperature indices (i.e., CSDI and TN10p). Concretely, the CSDI showed an ascent in the Greater Hinggan Mountains (G1), the Northeast Plain (G3), the Changbai Mountains (G4), the southern part of the Loess Plateau (G5), and parts of the Yangtze River Basin (G8). However, these trends were reversed in some other areas, including the Hainan Island, the Wuyi Mountain (G9), the East China Plain, and the Yangtze River Basin (G8). This result is consistent with Du (2015) [56]. The TN10p showed generally weak trends in the southern parts of the NSTEC. In addition, the trend of TN10p is consistent with that of the CSDI but different in magnitude. In terms of extreme high temperature indices (i.e., WSDI and TX90p), similar changes could be found between them (Figure 6d,e). In detail, the WSDI and TX90p showed increasing trends in most areas of the NSTEC. However, an obvious decrease in the WSDI could be found in the Northeast Plain.

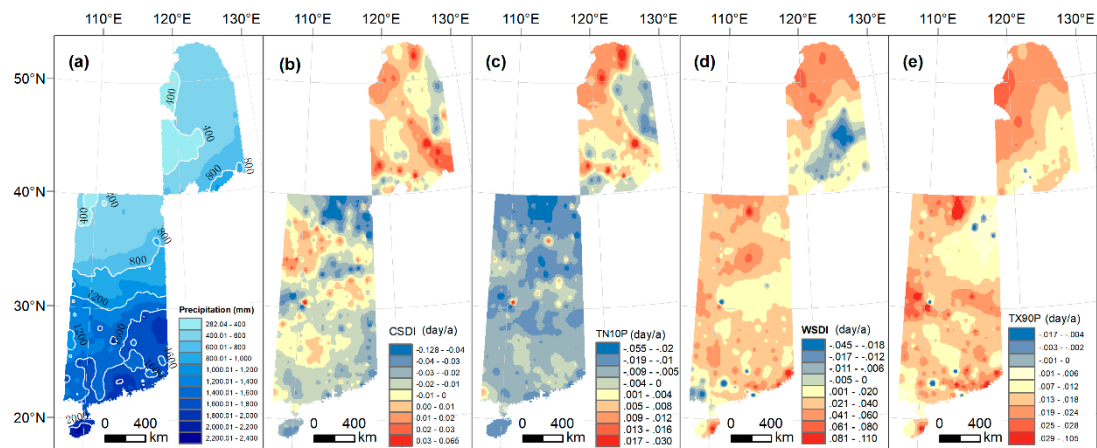


Figure 6. Spatial distribution of (a) mean precipitation, trends of (b) CSDI, (c) TN10p, (d) WSDI, and (e) TX90p from 1982 to 2012.

4.2.3. Intensity of Extreme Temperature and Precipitation Events

Figures 7 and 8 show the changes of extreme temperature intensity in the NSTEC from 1982 to 2012. In detail, the intensity of extreme cold temperature events (TNN) showed a fluctuation from 1982 to 2012 ($0.013 \pm 0.024 \text{ } ^\circ\text{C}\cdot\text{year}^{-1}$, $R^2 = 0.001$, $P = 0.966$). However, an enhanced warming trend could be found in Changbai Mountains and the northern parts of the North China Plain. For extreme high temperature events (TXX), small increasing trends could be found in the NSTEC over the past decades ($0.036 \pm 0.013 \text{ } ^\circ\text{C}\cdot\text{year}^{-1}$, $R^2 = 0.220$, $P = 0.634$).

An overall fluctuation was found for the extreme precipitation index (R95p) in the NSTEC from 1982 to 2012 ($4.3 \pm 8.4 \text{ mm}\cdot\text{year}^{-1}$, $R^2 = 0.009$, $P = 0.611$). The spatial distribution mainly showed a decreasing trend in the northern NSTEC. Both increasing and decreasing trends could be found in the southern NSTEC [57]. Precipitation may affect vegetation types deeply and even the NDVI because the main potential climatic constraints for plant growth are sunlight in the south, water in the middle, and temperature in the north of the NSTEC, according to Nemani et al. [58].

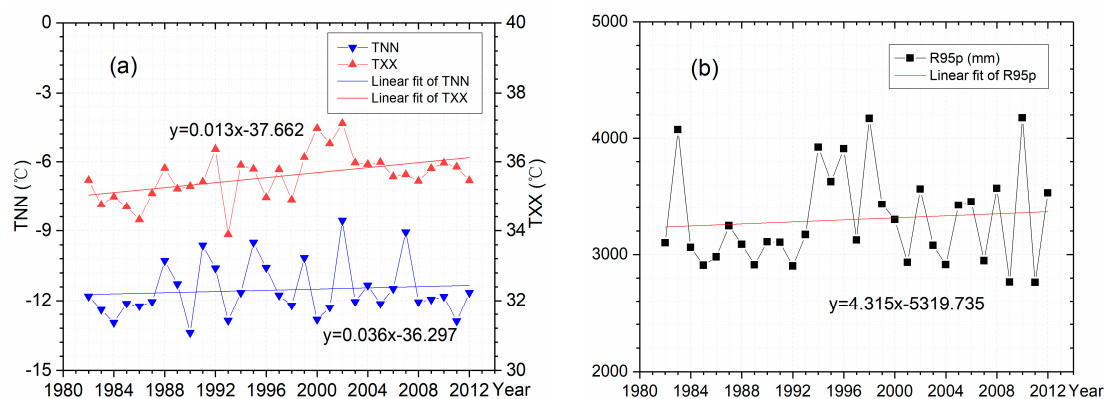


Figure 7. Temporal variations of the intensity indices of extreme climate events from 1982 to 2012: (a) TNN and TXX; (b) R95p.

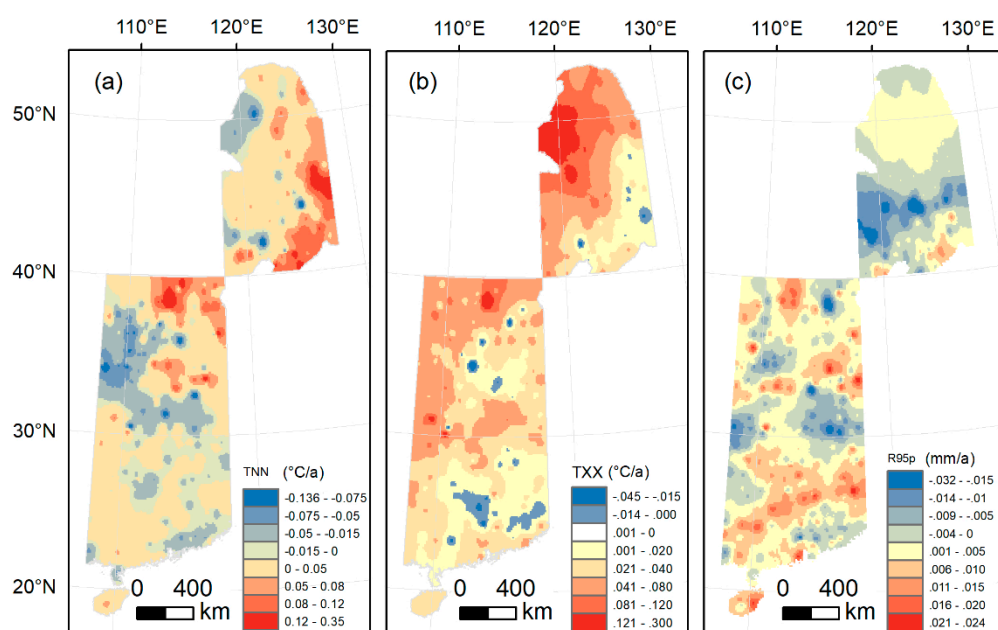


Figure 8. Spatial distribution of the trends of (a) TNN, (b) TXX, and (c) R95p from 1982 to 2012.

4.3. Correlations between the Indices of Extreme Climate Events and Vegetation Activity

4.3.1. Correlation between the Frequency Indices of Extreme Climate Events and Vegetation Activity

The correlations between frequency indices of extreme temperature events (i.e., CSDI, TN10p, WSDI, and TX90p) and NDVI were first analyzed over the period 1982–2012 in the NSTEC. Negative correlations could be found between the CSDI and the SWS-derived NDVI in 78% of the meteorological stations ($R < -0.1$; $P < 0.05$). Similar correlations could also be found in 74% of the meteorological stations when using GIMMS-3g-derived NDVI as variables ($R < -0.1$; $P < 0.05$). The TN10p showed negative correlations with the SWS-derived NDVI and GIMMS-3g NDVI in 81% and 73% of the stations, respectively. These results indicate that the frequency of extreme low temperature events, which are represented by the CSDI and the TN10p, were most negatively correlated with the NDVI during 1982–2012 in the NSTEC.

In addition, the frequency of extreme high temperature indices was positively correlated with the NDVI in most stations. According to the analysis of the SWS-derived NDVI and GIMMS-3g NDVI, 65% and 57% of the stations showed positive correlations between the WSDI and the two NDVI datasets at a 95% confidence level. Moreover, 70% and 88% of the TX90p stations showed significant positive correlations between the index and the two NDVI datasets ($R > 0.1$; $P < 0.05$).

Figure 9 shows the spatial distributions of the correlation between the frequency indices of extreme climate events and the NDVI datasets from the NOAA-SWS and GIMMS-3g. Similar patterns were found on the correlations between the two NDVI datasets and the frequency indices of extreme climate events. Concretely, the CSDI and the TN10p were negatively correlated with the NDVI in most stations in the Northeast Plain (G3) and the Yangtze River Basin (G8) in Figures 8e and 9a. As one of the main crop production areas, the NDVI for crop plants in the Northeast Plain was higher (or lower) when the number of consecutive days of cold temperature decreased (or increased) in past decades. These results could be due in part to the fact that crop plants are subject to suffering cold stress [59,60]. Further, crop growth may also be affected by irrigation [61] and soil erosion [62].

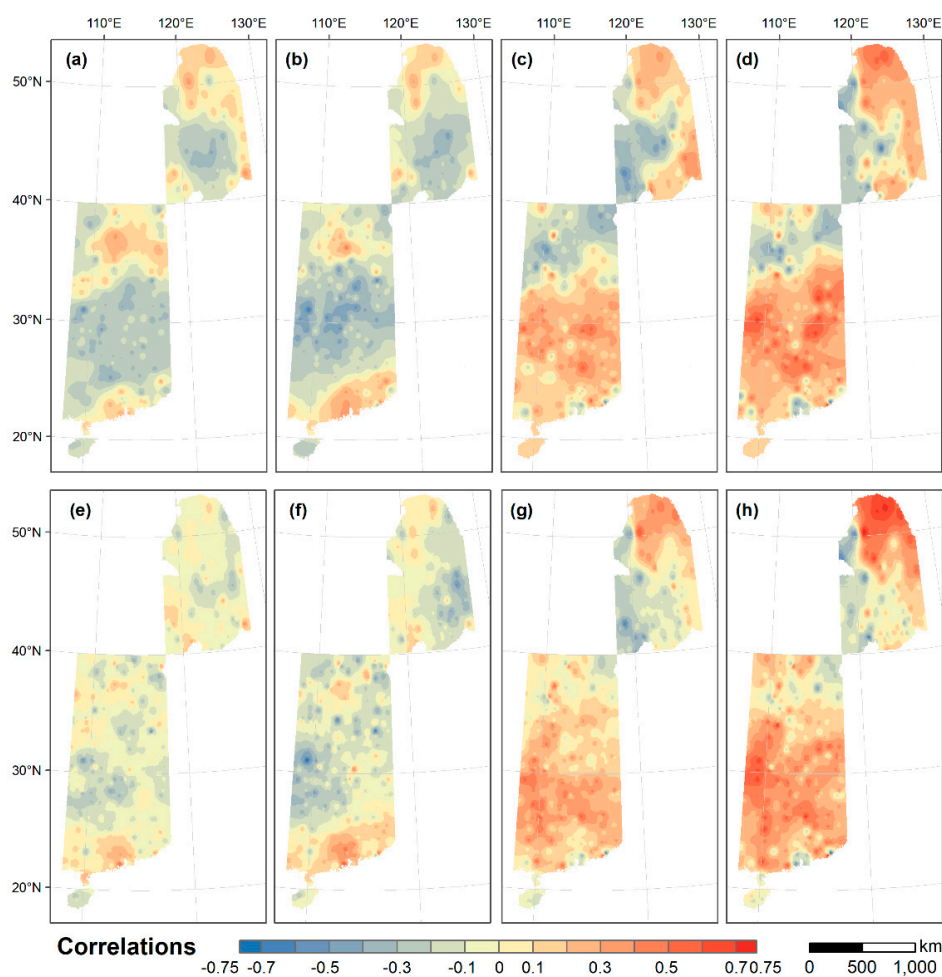


Figure 9. Correlations between the NOAA-SWS NDVI and (a) CSDI, (b) TN10p, (c) WSDI, and (d) TX90p, as well as between the GIMMS-3g NDVI and (e) CSDI, (f) TN10p, (g) WSDI, and (h) TX90p.

As shown in Figure 9c,g, positive correlations between the WSDI and the NDVI are mainly distributed in the eastern and southern parts of the NSTEC. This result indicates the possible enhancement of vegetation activity owing to the frequent occurrence of extreme high temperatures. In the southern NSTEC with a deciduous broad-leaved forest, concurrences of rain and heat energy provide favorable conditions for vegetation growth in monsoon climates. Similar phenomena could also be found in the northernmost part of the NSTEC, including the regions in the Changbai Mountain (G4) and the northern of Great Hinggan Mountains (G1) [63]. In addition, negative correlations could be found in the semi-arid areas where water is insufficient, including the Inner Mongolia Plateau (G2) and the Northeast Plain (G3) [63]. Negative correlations could be due to the fact that the vegetation growth of grasslands and croplands is inhibited, as extremely high temperatures can accelerate transpiration

and evapotranspiration and thus threaten vegetation growth [64]. Similar patterns could also be found between the TX90p and the NDVI (Figure 9d,h).

4.3.2. Correlation between the Intensity Indices of Extreme Climate Events and Vegetation Activity

For extreme high temperature intensities, most stations passed a significance test according to the correlation analysis between the TXX and the NDVI. Among them, 63% and 50% of the stations showed positive correlations ($R > 0.1$; $P < 0.05$) according to the analysis of the SWS-derived NDVI and GIMMS-3g NDVI. For the extreme cold temperature intensity (TNN), we found that 53% and 63% of the stations showed a positive correlation between the TNN and the two NDVI datasets, respectively.

As shown in Figure 10, consistent correlations could be found between the two satellite-derived NDVI observations and the intensity indices of extreme climate events (i.e., TNN, TXX, and R95p). That is, the correlation between extreme high temperature and NDVI is mainly positive in the northeast and south parts of the NSTEC. In addition, the correlation between the NDVI and the TXX is highly consistent with that of the WSDI and the TX90p (Figure 9c,d,g,h and Figure 10b). However, for extreme cold temperature intensity, the spatial distribution of the correlation between the NDVI and the TNN was different from that of the frequency of extreme cold temperature events. In detail, the TNN was positively correlated with the NDVI in most of the NSTEC.

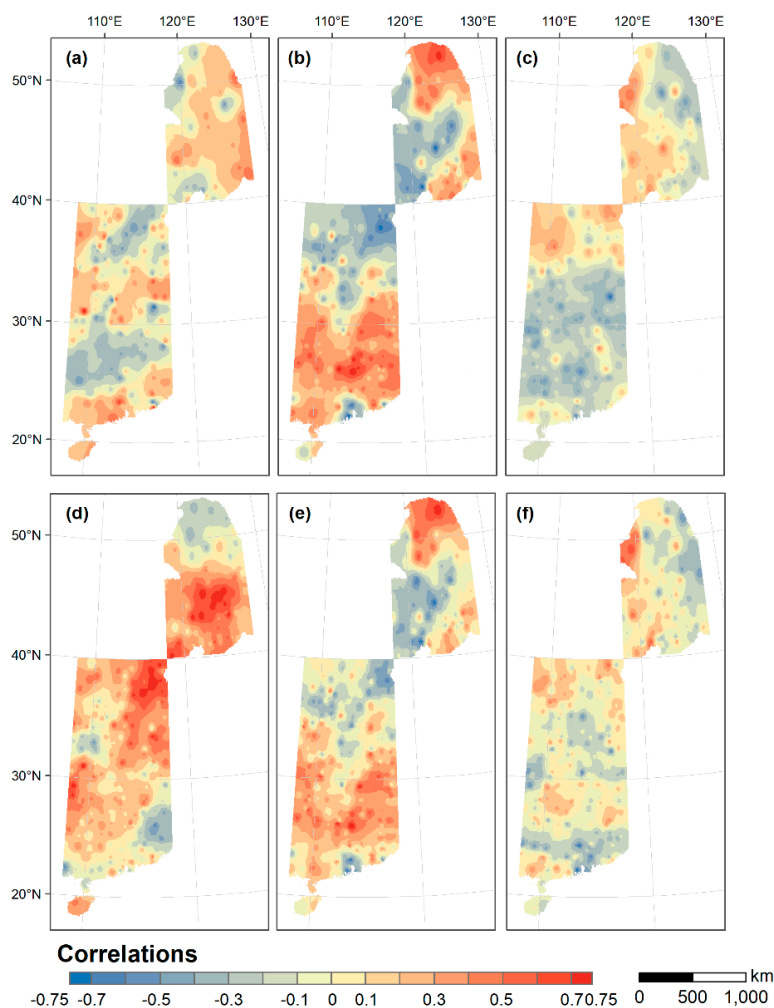


Figure 10. Correlations between the NOAA-SWS-derived NDVI and (a) TNN, (b) TXX, and (c) R95p, as well as between the GIMMS-3g-derived NDVI and (d) TNN, (e) TXX, and (f) R95p.

For extreme precipitation intensity, negative correlations between the R95p and the NDVI were widely found in the Yangtze Basin, the Pearl River Basin, and the northernmost of the NSTEC. On the other hand, the positive correlations between R95p and NDVI were mainly concentrated in the central region of the NSTEC (Figure 10c,f), such as the Loess Plateau (G5), the Inner Mongolia Plateau (G2), and the Northeast Plain (G3). This phenomenon could be due to the fact that rainstorms can promote vegetation growth in the water-limited conditions in semi-arid regions [65].

The effect of extreme climate events on the NDVI were also analyzed by combining the frequency and intensity of extreme climate events as a whole. For instance, both the frequency and intensity of extreme high temperature indices (i.e., WSDI, TX90p, and TXX) showed overall increasing trends in the past decades in the NSTEC (Figures 5 and 7). Accordingly, the NDVI revealed an enhanced trend during this period. Furthermore, an obvious negative effect of extreme climate events on vegetation activity could be found in 1984, 1993, 2000, 2005, and 2007 (Table 2). For instance, the frequency and intensity of extreme cold temperatures (i.e., CSDI, TN10p, and TNN) were relatively severe in 1984. That is, extreme cold temperature events occurred more frequently and lasted for a longer time than during any other periods. Consequently, the NDVI showed a lower level than in any other years. Similar phenomena could also be found in 2005.

Table 2. Changes of the NDVI and the extreme climate indices when severe extreme climate events occurred (where +/- represents the fact that extreme climate indices are higher/lower than usual).

Year	Higher than Usual	Lower than Usual	NDVI-SWS	NDVI-GIMMS
1984	CSDI, TN10p, TNN		-	-
1993	CSDI, TN10p	TNN, WSDI, TX90p, TXX	-	-
2000	TX90p, TXX	R95p	-	-
2005	CSDI, TN10p, TNN		-	-
2007	TNN, TX90p	CSDI, TN10p	+	+

In 1993, the frequency of extreme cold temperature events (e.g., CSDI and TN10p) was increased, while the intensity of the extreme cold temperature events was strengthened (Table 2). As a result, the NDVI was relatively small due to the frequent occurrence of severe extreme cold temperatures. In 2000, both the frequency and intensity of extreme high temperatures were found to be enhanced (i.e., a large TX90p and large TXX). Meanwhile, a weak intensity for extreme precipitation events was found in the NSTEC (Figure 5). Consequently, the NDVI was relatively small in comparison with that during other periods. This NDVI reduction could be attributed to the large-scale droughts in the region [66]. In 2007, the frequency and intensity of extreme cold temperature events were relatively weak (i.e., a small CSDI, small TN10p, and high TNN). Thus, the NDVI was relatively high in that period.

We further explored the combined spatial effects of the frequency and intensity of extreme climate events on vegetation in the NSTEC. Three typical regions were then analyzed: A1, a water-limited area; A2, a monsoon climate zone; and A3, an urbanized area (Figure 11). In detail, In the region A1, extreme precipitation events showed a weakening trend (Figure 11e). Meanwhile, we found concurrent occurrences of increased frequency, as well as enhanced intensity of extreme high/cold temperatures (Figure 11b–d,f–h). Consequently, the NDVI showed mainly weakening trends over the past decades. Nevertheless, the NDVI showed an increasing trend in the northern Greater Hinggan Mountains (G1). This increase could be associated with the obvious increase in the days of the biological growth season [67], as well as the wide distribution of forest lands, including coniferous forests and coniferous mixed forests. In region A2, the NDVI mainly showed an upward trend (e.g., Jiangnan-Dongting-Lake Plain; G7 in Figure 11). This increased NDVI could be associated with the abundant moisture and heat in a typical monsoon climate. Concretely, the intensity and frequency of extreme high temperatures increased significantly, while extreme precipitation revealed overall increasing trends. In addition, the intensity and frequency of extreme cold temperatures showed decreasing trends. Consequently, the concurrences of rain and heat energy provided a suitable environment for plant growth. A3 is mainly

located in the Pearl River Delta (G10). In this region, the NDVI decreases significantly. This decrease could be mainly associated with rapid urban expansion in past decades. Since the 1980s, urbanization in the Pearl River Delta has increased by more than 60% [68]. Although the frequency and intensity of extreme high temperatures increased significantly in A3, the increase of urban land use will lead to a significant reduction in vegetation activity [69].

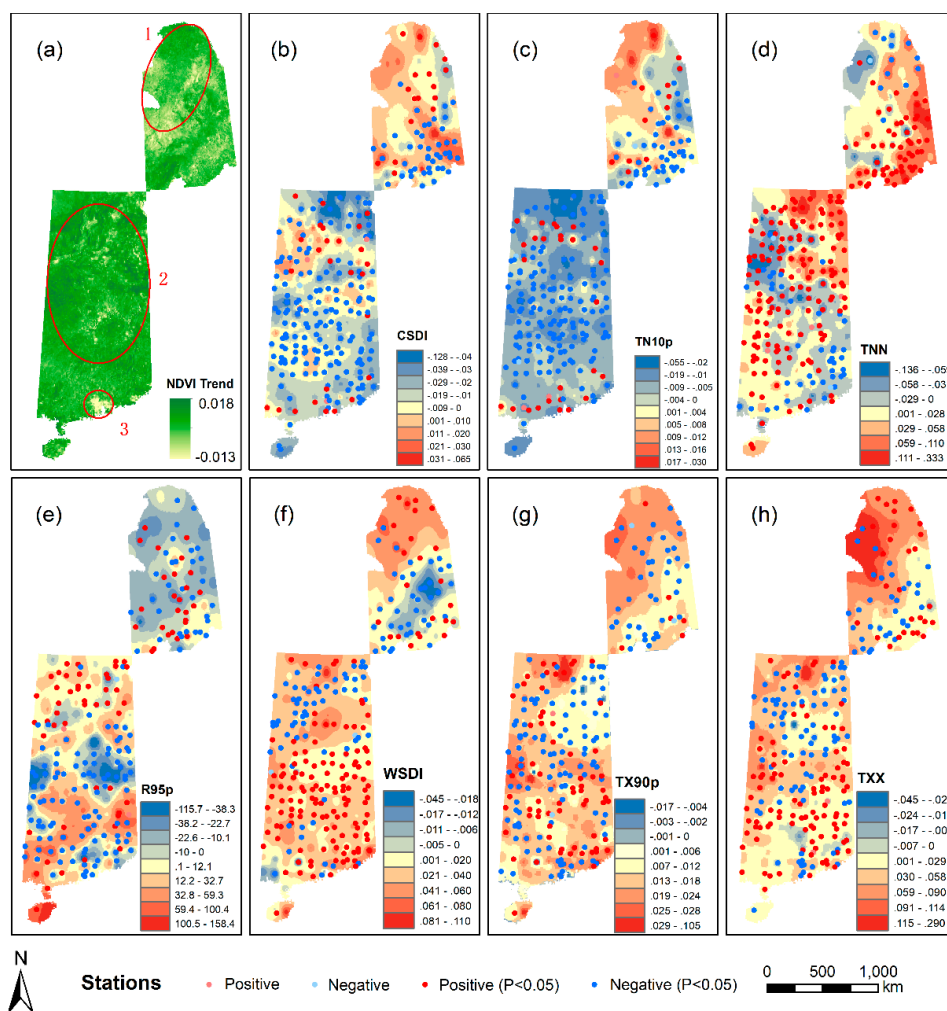


Figure 11. The trends of the mean NDVI and seven extreme climate indices, as well as the correlations among them by stations (a: NDVI, b: CSDI, c: TN10p, d: TNN, e: R95p, f: WSDI, g: TX90p, and h: TXX).

4.3.3. Analysis of the Correlation between Different Climatic Ecozones

As shown in Table 3, consistent correlations could be found in most cases from both the NOAA-SWS and GIMMS-3g datasets. For instances, extreme temperature events mainly showed positive effects on cold temperate coniferous forests. In addition, temperate grasslands are affected by extreme cold temperature events. That is, the frequency of extreme cold temperature mainly has negative relationships with NDVI. That is, more extreme cold temperature events could reduce the NDVI in temperate grasslands. Extreme high temperature indices (i.e., TXX, WSDI and TX90p) mainly have a negative effect on grasslands. In addition, extreme precipitation events have a positive influence on the grassland according to both satellite-derived observations (likely induced by the watering effects in semi-arid areas).

Table 3. Correlation between the NDVI and extreme climate indices by ecozones (SWS and GIMMS represent the NDVI from NOAA-SWS and GIMMS-3g).

Ecozone	Data Source	Correlation						
		TNN	CSDI	TN10p	TXX	WSDI	TX90p	R95p
Tropical monsoon rainforest	SWS	0.220	−0.171	0.249	−0.263	0.199	−0.297	−0.221
	GIMMS	0.295	−0.232	−0.294	0.208	0.352	0.412	−0.224
Subtropical evergreen broad-leaved forest	SWS	0.252	−0.230	−0.281	0.269	0.272	0.342	−0.284
	GIMMS	0.260	−0.261	−0.248	0.244	0.251	0.254	−0.257
Warm-temperate deciduous broad-leaved forest	SWS	0.349	−0.208	−0.245	−0.288	−0.287	−0.291	0.241
	GIMMS	−0.232	−0.274	−0.281	−0.256	−0.265	−0.223	0.223
Temperate mixed forest	SWS	0.334	−0.222	−0.304	0.245	0.282	0.273	−0.315
	GIMMS	−0.222	−0.217	−0.235	0.231	0.208	−0.241	−0.212
Temperate grassland	SWS	0.356	−0.259	−0.255	−0.294	−0.296	0.258	0.259
	GIMMS	−0.219	0.259	−0.215	−0.235	−0.275	−0.286	0.287
Cold temperate coniferous forest	SWS	−0.203	0.266	0.212	0.383	0.248	0.432	−0.220
	GIMMS	0.218	0.200	−0.213	0.349	0.268	−0.268	−0.219

For forest vegetation, including temperate mixed forests and subtropical evergreen broad-leaved forests, relatively consistent correlations could be found from both the NOAA-SWS and GIMMS-3g observations. For temperate mixed forests, subtropical evergreen broad-leaved forests, and tropical monsoon rainforests, both the frequency and intensity of extreme high temperature have positive effects on vegetation. In addition, extreme precipitation events had negative effects on the vegetation.

On the other hand, the NDVIs are positively correlated with the extreme precipitation index in warm-temperate deciduous broad-leaved forests. Furthermore, both the intensity and frequency of extreme high temperature have a negative effect on vegetation growth.

4.4. Possible Causes of the Vegetation Activity Changes to Extreme Climate Events

According to the aforementioned results, the vegetation NDVI reveals an overall increasing trend in the NSTEC from 1982 to 2012, even though spatial heterogeneity exists. This increase could be associated with extreme climate characteristics, vegetation types, and human activities. For instance, the vegetation growth of grasslands and croplands could be inhibited by changes in extreme high temperature events and extreme precipitation events in the Inner Mongolia Plateau and the Northeast Plain [32]. Similar results were also found in the case study of European in Baumbach et al. [70].

In addition, human activities, including urban land development, could dramatically affect local vegetation activity. One of the typical examples is in the Pearl River Delta. Despite favorable climate conditions, vegetation activity in this region still decreased in past decades. The main reason for this phenomenon could be attributed to large urban land development.

Furthermore, climate change, especially the combined effects of extreme precipitation events, as well as the frequency and intensity of extreme temperature events, could be attributed to changes in vegetation activity. For instance, vegetation activity revealed increasing trends in the Jiangnan-Dongting-Lake Plain, the Yangtze River Basin, and the Wuyishan District due to the concurrent occurrences of enhanced high temperature extremes, precipitation extremes, and weakened cold temperature extremes.

5. Conclusions

Transect analysis has obvious advantages on understanding the effects of climate change on terrestrial vegetation activity by substituting space for time [25,26]. In this paper, the impacts of extreme climate events on vegetation activity were assessed over the period of 1982–2012 using the North South Transect of Eastern China (NSTEC) as a case study. Seven extreme climate indices from ETCCDI were selected to reflect changes of extreme climate events from aspects of frequency and intensity. We

found that the frequency and the intensity of extreme high temperatures events showed an overall enhanced trend. However, we also found an enhanced frequency and weakened intensity of extreme cold temperature events, although they were not significant. Under such conditions, vegetation activity revealed an overall strengthened trend in the NSTEMC over the past decades. Despite this, this trend is locally uncertain. The possible causes of the vegetation activity changes to extreme climate events were explored from the perspectives of vegetation type and human activity, as well as the combined effects of precipitation extremes and the frequency and intensity of temperature extremes.

This paper highlights the necessity to clarify the vital role of climate extremes on vegetation activity. However, there are also limitations in this study. For instances, vegetation activity was captured using NDVI as an indicator. Nevertheless, the NDVI still has some limitations. For example, it is easily saturated in rainforest areas and is susceptible to water vapor, dust aerosol pollution, and so on [30]. In addition, uncertainties still exist when sampling the NDVI based on meteorological stations from satellite-derived datasets at a coarse resolution. In addition, extreme climate events are frequently instantaneous and often exert severe influences on vegetation growth during a certain period. However, vegetation responses to extreme climate events are often lagged [71–73]. The lag time period is still uncertain due to the differences in vegetation type, as well as the magnitude, duration, and frequency of extreme climate events. Consequently, the impacts of extreme climate events on vegetation activity deserve further investigation by tacking them with different lag time periods in the future.

Author Contributions: F.P. contributed to the research design, data analysis, interpretation of results, and draft manuscript preparation; Y.Z. and F.P. contributed to the data collection; Y.Z. performed experiments and computational analysis; Y.X., C.W., K.W., H.W., R.Z., and Y.C. assisted with the experiments; F.P. and Y.Z. drafted the paper, and all authors contributed to the final draft of the manuscript.

Funding: This research was funded by the National Natural Science Foundation of China (Grant No. 41401438), the Postgraduate Research and Practice Innovation Program of Jiangsu Province (Grant No. KYCX18_2121), the Priority Academic Program Development of Jiangsu Higher Education Institutions, and the National Students' Project for Innovation Training Program of China (Grant No. 201810320020Z).

Acknowledgments: The authors thank the National Climate Center, China Meteorological Administration, and Data Center for Resources and Environmental Sciences, Chinese Academy of Sciences for providing the meteorological data, climate zones, vegetation types, and elevation data for this study. We are very grateful to the reviewers for their constructive comments and thoughtful suggestions.

Conflicts of Interest: The authors declare no conflict of interest.

References

1. Shen, Y.; Wang, G. Key findings and assessment results of IPCC WGI fifth assessment report. *J. Glaciol. Geocryol.* **2013**, *35*, 1068–1076.
2. Alexander, L.; Allen, S.; Nathaniel, L. *Climate Change 2013: The Physical Science Basis Summary for Policymakers*; Intergovernmental Panel on Climate Change: Geneva, Switzerland, 2013.
3. Ciais, P.; Reichstein, M.; Viovy, N.; Granier, A.; Ogee, J.; Allard, V.; Aubinet, M.; Buchmann, N.; Bernhofer, C.; Carrara, A. Europe-wide reduction in primary productivity caused by the heat and drought in 2003. *Nature* **2005**, *437*, 529–533. [[CrossRef](#)] [[PubMed](#)]
4. Heisler-White, J.L.; Blair, J.M.; Kelly, E.F.; Harmoney, K.; Knapp, A.K. Contingent productivity responses to more extreme rainfall regimes across a grassland biome. *Glob. Chang. Biol.* **2009**, *15*, 2894–2904. [[CrossRef](#)]
5. Taylor, R.G.; Scanlon, B.; Döll, P.; Rodell, M.; Beek, R.V.; Wada, Y.; Longuevergne, L.; Leblanc, M.; Famiglietti, J.S.; Edmunds, M. Ground water and climate change. *Nat. Clim. Chang.* **2013**, *3*, 322–329. [[CrossRef](#)]
6. Pei, F.; Wu, C.; Liu, X.; Hu, Z.; Xia, Y.; Liu, L.A.; Wang, K.; Zhou, Y.; Xu, L. Detection and attribution of extreme precipitation changes from 1961 to 2012 in the Yangtze River Delta in China. *Catena* **2018**, *169*, 183–194. [[CrossRef](#)]
7. Brown, M.E.; Pinzon, J.E.; Didan, K.; Morisette, J.T.; Tucker, C.J. Evaluation of the consistency of long-term NDVI time series derived from AVHRR, SPOT-vegetation, SeaWiFS, MODIS, and Landsat ETM+ sensors. *IEEE Trans. Geosci. Remote Sens.* **2006**, *44*, 1787–1793. [[CrossRef](#)]

8. Lange, M.; Dechant, B.; Rebmann, C.; Vohland, M.; Cuntz, M.; Doktor, D. Validating MODIS and Sentinel-2 NDVI Products at a Temperate Deciduous Forest Site Using Two Independent Ground-Based Sensors. *Sensors* **2017**, *17*, 1855. [[CrossRef](#)]
9. Beck, H.E.; McVicar, T.R.; van Dijk, A.I.J.M.; Schellekens, J.; de Jeu, R.A.M.; Bruijnzeel, L.A. Global evaluation of four AVHRR–NDVI data sets: Intercomparison and assessment against Landsat imagery. *Remote Sens. Environ.* **2011**, *115*, 2547–2563. [[CrossRef](#)]
10. Zhang, Y.; Zhu, Z.; Liu, Z.; Zeng, Z.; Ciais, P.; Huang, M.; Liu, Y.; Piao, S. Seasonal and interannual changes in vegetation activity of tropical forests in Southeast Asia. *Agric. For. Meteorol.* **2016**, *224*, 1–10. [[CrossRef](#)]
11. Wu, D.; Zhao, X.; Liang, S.; Zhou, T.; Huang, K.; Tang, B.; Zhao, W. Time-lag effects of global vegetation responses to climate change. *Glob. Chang. Biol.* **2015**, *21*, 3520–3531. [[CrossRef](#)]
12. Tian, H.; Cao, C.; Wei, C.; Bao, S.; Yang, B.; Myneni, R.B. Response of vegetation activity dynamic to climatic change and ecological restoration programs in Inner Mongolia from 2000 to 2012. *Ecol. Eng.* **2015**, *82*, 276–289. [[CrossRef](#)]
13. Cai, D.; Fraedrich, K.; Sielmann, F.; Guan, Y.; Shan, G.; Ling, Z.; Zhu, X. Climate and vegetation: An ERA-Interim and GIMMS NDVI analysis. *J. Clim.* **2014**, *27*, 5111–5118. [[CrossRef](#)]
14. Barichivich, J.; Briffa, K.R.; Myneni, R.B.; Osborn, T.J.; Melvin, T.M.; Philippe, C.; Shilong, P.; Compton, T. Large-scale variations in the vegetation growing season and annual cycle of atmospheric CO₂ at high northern latitudes from 1950 to 2011. *Glob. Chang. Biol.* **2013**, *19*, 3167–3183. [[CrossRef](#)] [[PubMed](#)]
15. Zhou, L.; Tucker, C.J.; Kaufmann, R.K.; Slayback, D.; Shabanov, N.V.; Myneni, R.B. Variations in northern vegetation activity inferred from satellite data of vegetation index during 1981 to 1999. *J. Geophys. Res. Atmos.* **2001**, *106*, 20069–20083. [[CrossRef](#)]
16. Felton, A.J.; Smith, M.D. Integrating plant ecological responses to climate extremes from individual to ecosystem levels. *Philos. Trans. R. Soc. Lond. B Biol. Sci.* **2017**, *372*, 20160142. [[CrossRef](#)]
17. Reyer, C.P.O.; Brouwers, N.; Rammig, A.; Brook, B.W.; Epila, J.; Grant, R.F.; Holmgren, M.; Langerwisch, F.; Leuzinger, S.; Lucht, W. Forest resilience and tipping points at different spatio-temporal scales: Approaches and challenges. *J. Ecol.* **2015**, *103*, 5–15. [[CrossRef](#)]
18. Tan, Z.; Tao, H.; Jiang, J.; Zhang, Q. Influences of Climate Extremes on NDVI (Normalized Difference Vegetation Index) in the Poyang Lake Basin, China. *Wetlands* **2015**, *35*, 1033–1042. [[CrossRef](#)]
19. Sarmah, S.; Jia, G.; Zhang, A.; Singha, M. Assessing seasonal trends and variability of vegetation growth from NDVI3g, MODIS NDVI and EVI over South Asia. *Remote Sens. Lett.* **2018**, *9*, 1195–1204. [[CrossRef](#)]
20. Zhao, A.; Zhang, A.; Liu, X.; Cao, S. Spatiotemporal changes of normalized difference vegetation index (NDVI) and response to climate extremes and ecological restoration in the Loess Plateau, China. *Theor. Appl. Climatol.* **2018**, *132*, 555–567. [[CrossRef](#)]
21. Yao, J.; Chen, Y.; Zhao, Y.; Mao, W.; Xu, X.; Liu, Y.; Yang, Q. Response of vegetation NDVI to climatic extremes in the arid region of Central Asia: A case study in Xinjiang, China. *Theor. Appl. Climatol.* **2017**, *131*, 1503–1515. [[CrossRef](#)]
22. Li, C.; Wang, J.; Hu, R.; Yin, S.; Bao, Y.; Ayal, D.Y. Relationship between vegetation change and extreme climate indices on the Inner Mongolia Plateau, China, from 1982 to 2013. *Ecol. Indic.* **2018**, *89*, 101–109. [[CrossRef](#)]
23. Mélin, F.; Sclep, G.; Jackson, T.; Sathyendranath, S. Uncertainty estimates of remote sensing reflectance derived from comparison of ocean color satellite data sets. *Remote Sens. Environ.* **2016**, *177*, 107–124. [[CrossRef](#)]
24. Julien, Y.; Sobrino, J.A. Comparison of cloud-reconstruction methods for time series of composite NDVI data. *Remote Sens. Environ.* **2010**, *114*, 618–625. [[CrossRef](#)]
25. Li, Y.; Liao, S.; Chi, G.; Liao, Q. NPP distribution related to the terrains along the North-South Transect of Eastern China. *Sci. Bull.* **2004**, *49*, 617–624. [[CrossRef](#)]
26. Sheng, W.; Ren, S.; Yu, G.; Fang, H.; Jiang, C.; Mi, Z. Patterns and driving factors of WUE and NUE in natural forest ecosystems along the North-South Transect of Eastern China. *J. Geogr. Sci.* **2011**, *21*, 651–665. [[CrossRef](#)]
27. Tucker, C.J.; Pinzon, J.E.; Brown, M.E.; Slayback, D.A.; Pak, E.W.; Mahoney, R.; Vermote, E.F.; Saleous, N.E. An extended AVHRR 8 km NDVI dataset compatible with MODIS and SPOT vegetation NDVI data. *Int. J. Remote Sens.* **2005**, *26*, 4485–4498. [[CrossRef](#)]
28. Zhu, X.; Yu, G.; He, H. *Radiation and Light-Use Efficiency Dataset of Typical Chinese Ecosystems (2002–2010)*; China Scientific Data: Beijing, China, 2018.

29. CMA. *Surface Meteorological Observation Standards*; China Meteorological Press: Beijing, China, 1979; pp. 167–192. (In Chinese)
30. Richardson, A.J. Distinguishing vegetation from soil background information. *Photogramm. Eng. Remote Sens.* **1977**, *43*, 1541–1552.
31. Tucker, C.J. Red and photographic infrared linear combinations for monitoring vegetation. *Remote Sens. Environ.* **1979**, *8*, 127–150. [[CrossRef](#)]
32. Justice, C.O.; Townshend, J.R.G.; Holben, B.N.; Tucker, C.J. Analysis of the phenology of global vegetation using meteorological satellite data. *Int. J. Remote Sens.* **1985**, *6*, 1271–1318. [[CrossRef](#)]
33. Pei, F.; Wu, C.; Liu, X.; Xia, L.; Yang, K.; Yi, Z.; Wang, K.; Li, X.; Xia, G. Monitoring the vegetation activity in China using vegetation health indices. *Agric. For. Meteorol.* **2018**, *248*, 215–227. [[CrossRef](#)]
34. Silva, F.B.; Shimabukuro, Y.E.; Aragao, L.E.; Anderson, L.O.; Pereira, G.; Cardozo, F.; Arai, E. Large-scale heterogeneity of Amazonian phenology revealed from 26-year long AVHRR/NDVI time-series. *Environ. Res. Lett.* **2013**, *8*, 24011. [[CrossRef](#)]
35. Vrieling, A.; Hoedjes, J.C.; van der Velde, M. Large-Scale Assessment of Soil Erosion in Africa: Satellites Help to Jointly Account for Dynamic Rainfall and Vegetation Cover. In Proceedings of the EGU General Assembly Conference Abstracts, Vienna, Austria, 12–17 April 2015.
36. Liu, Y.; Li, Y.; Li, S.; Motesharrei, S. Spatial and temporal patterns of global NDVI trends: Correlations with climate and human factors. *Remote Sens.* **2015**, *7*, 13233–13250. [[CrossRef](#)]
37. Tourre, Y.M.; Jarlan, L.; Lacaux, J.P.; Rotela, C.H.; Lafaye, M. Spatio-temporal variability of NDVI-precipitation over southernmost South America: Possible linkages between climate signals and epidemics. *Environ. Res. Lett.* **2008**, *3*, 52–55. [[CrossRef](#)]
38. Piao, S.; Fang, J.; Zhou, L.; Guo, Q.; Henderson, M.; Ji, W.; Li, Y.; Tao, S. Interannual variations of monthly and seasonal normalized difference vegetation index (NDVI) in China from 1982 to 1999. *J. Geophys. Res.* **2003**, *108*, 4401. [[CrossRef](#)]
39. Fang, J.; Shilong, P. Increasing terrestrial vegetation activity in China, 1982–1999. *Sci. China* **2004**, *47*, 229–240.
40. Thoma, D.P.; Montagne, C. Short-Term Monitoring of Rangeland Forage Conditions with AVHRR Imagery. *J. Range Manag.* **2002**, *55*, 383–389. [[CrossRef](#)]
41. Lamchin, M.; Park, T.; Lee, J.Y.; Lee, W.K. Monitoring of Vegetation Dynamics in the Mongolia Using MODIS NDVIs and their Relationship to Rainfall by Natural Zone. *J. Indian Soc. Remote* **2015**, *43*, 325–337. [[CrossRef](#)]
42. R Core Team. *R: A Language and Environment for Statistical Computing [Computer Software Manual]*; R Foundation for Statistical Computing: Vienna, Austria, 2011.
43. Pohlert, T. *Non-Parametric Trend Tests and Change-Point Detection*. CC BY-ND 4. 2018. Available online: <https://cran.r-project.org/web/packages/trend/> (accessed on 1 November 2019).
44. Ren, G.; Chen, Y.; Zou, X.; Zhou, Y.; Wang, X.; Jiang, Y.; Ren, F. Definition and Trend Analysis of an Integrated Extreme Climatic Index. *Clim. Environ. Res.* **2010**, *15*, 354–364.
45. Frich, P.; Alexander, L.V.; Della-Marta, P.; Gleason, B.; Haylock, M.; Tank, A.M.G.K.; Peterson, T. Observed coherent changes in climatic extremes during 2nd half of the 20th century. *Clim. Res.* **2002**, *19*. [[CrossRef](#)]
46. Zhang, X.; Alexander, L.; Hegerl, G.C.; Jones, P.; Tank, A.K.; Peterson, T.C.; Trewin, B.; Zwiers, F.W. Indices for monitoring changes in extremes based on daily temperature and precipitation data. *Wiley Interdiscip. Rev. Clim. Chang.* **2011**, *2*, 851–870. [[CrossRef](#)]
47. Alexander, L.V. Global observed long-term changes in temperature and precipitation extremes: A review of progress and limitations in IPCC assessments and beyond. *Weather Clim. Extrem.* **2016**, *11*, 4–16. [[CrossRef](#)]
48. Peterson, T.C.; Manton, M.J. Monitoring changes in climate extremes: A tale of international collaboration. *Bull. Am. Meteorol. Soc.* **2008**, *89*, 1266–1271. [[CrossRef](#)]
49. Manton, M.J.; Della-Marta, P.M.; Haylock, M.R.; Hennessy, K.J.; Nicholls, N.; Chambers, L.E.; Collins, D.A.; Daw, G.; Finet, A.; Gunawan, D. Trends in extreme daily rainfall and temperature in Southeast Asia and the South Pacific: 1961–1998. *Int. J. Climatol.* **2001**, *21*, 269–284. [[CrossRef](#)]
50. Sheikh, M.M.; Manzoor, N.; Ashraf, J.; Adnan, M.; Collins, D.; Hameed, S.; Manton, M.J.; Ahmed, A.U.; Baidya, S.K.; Borgaonkar, H.P. Trends in extreme daily rainfall and temperature indices over South Asia. *Int. J. Climatol.* **2015**, *35*, 1625–1637. [[CrossRef](#)]
51. Worku, G.; Teferi, E.; Bantider, A.; Dile, Y.T. Observed changes in extremes of daily rainfall and temperature in Jemma Sub-Basin, Upper Blue Nile Basin, Ethiopia. *Theor. Appl. Climatol.* **2019**, *135*, 839–854. [[CrossRef](#)]

52. Chen, J.M.; Black, T.A. Defining Leaf-Area Index for Non-Flat Leaves. *Agric. For. Meteorol.* **1992**, *15*, 421–429. [[CrossRef](#)]
53. Garrigues, S.; Lacaze, R.; Baret, F.; Morisette, J.T.; Weiss, M.; Nickeson, J.E.; Fernandes, R.; Plummer, S.; Shabanov, N.V.; Myneni, R.B. Validation and intercomparison of global Leaf Area Index products derived from remote sensing data. *J. Geophys. Res. Biogeosci.* **2015**, *113*, 1010–1029. [[CrossRef](#)]
54. Fensholt, R.; Proud, S.R. Evaluation of Earth Observation based global long term vegetation trends—Comparing GIMMS and MODIS global NDVI time series. *Remote Sens. Environ.* **2012**, *119*, 131–147. [[CrossRef](#)]
55. Shu, S.J.; Yuan, W.; Xiong, A.Y. Estimation and analysis for geographic and orographic influences on precipitation distribution in China. *Chin. J. Geophys.* **2007**, *50*, 1482–1493. [[CrossRef](#)]
56. Du, H. Research on the Extreme Climate Events over Northeast China under Global Climate Change. Ph.D. Thesis, Northeast Normal University, Changchun, China, 2015.
57. Peng, Y.; Zhao, X.; Wu, D.; Tang, B.; Xu, P.; Du, X.; Wang, H. Spatiotemporal variability in extreme precipitation in China from observations and projections. *Water-Sui* **2018**, *10*, 1089. [[CrossRef](#)]
58. Nemani, R.R.; Keeling, C.D.; Hashimoto, H.; Jolly, W.M.; Piper, S.C.; Tucker, C.J.; Myneni, R.B.; Running, S.W. Climate-driven increases in global terrestrial net primary production from 1982 to 1999. *Science* **2003**, *300*, 1560–1563. [[CrossRef](#)] [[PubMed](#)]
59. Chinnusamy, V.; Zhu, J.; Zhu, J. Cold stress regulation of gene expression in plants. *Trends Plant Sci.* **2007**, *12*, 444–451. [[CrossRef](#)] [[PubMed](#)]
60. Thakur, P.; Kumar, S.; Malik, J.A.; Berger, J.D.; Nayyar, H. Cold stress effects on reproductive development in grain crops: An overview. *Environ. Exp. Bot.* **2010**, *67*, 429–443. [[CrossRef](#)]
61. Benli, B.; Pala, M.; Stockle, C.; Oweis, T. Assessment of winter wheat production under early sowing with supplemental irrigation in a cold highland environment using CropSyst simulation model. *Agric. Water Manag.* **2007**, *93*, 45–53. [[CrossRef](#)]
62. Pimentel, D. Soil Erosion: A Food and Environmental Threat. *Environ. Dev. Sustain.* **2006**, *8*, 119–137. [[CrossRef](#)]
63. Clifford, M.J.; Royer, P.D.; Cobb, N.S.; Breshears, D.D.; Ford, P.L. Precipitation thresholds and drought-induced tree die-off: Insights from patterns of *Pinus edulis* mortality along an environmental stress gradient. *New Phytol.* **2013**, *200*, 413–421. [[CrossRef](#)]
64. Li, X.; Li, X.; Chen, Y.H. Temporal responses of vegetation to climate variables in temperate steppe of northern China. *J. Plant Ecol.* **2007**, *31*, 1054–1062.
65. Yan, D.; Xu, T.; Girma, A.; Yuan, Z.; Weng, B.; Qin, T.; Do, P.; Yuan, Y. Regional correlation between precipitation and vegetation in the Huang-Huai-Hai River Basin, China. *WATER-SUI* **2017**, *9*, 557. [[CrossRef](#)]
66. Yu, C. Features of Weather/Climate over China in 2000. *Meteorol. Mon.* **2001**, *4*, 20–24. (In Chinese)
67. Yang, X.; Lin, E.; Ma, S.; Ju, H.; Guo, L.; Xiong, W.; Li, Y.; Xu, Y. Adaptation of agriculture to warming in Northeast China. *Clim. Chang.* **2007**, *84*, 45–58. [[CrossRef](#)]
68. Xu, X.; Li, X. Review and preview of the urbanization in pearl river delta in the past 30 years of reform and opening up. *Econ. Geogr.* **2009**, *29*, 13–18.
69. Pei, F.; Li, X.; Liu, X.; Lao, C.; Xia, G. Exploring the response of net primary productivity variations to urban expansion and climate change: A scenario analysis for Guangdong Province in China. *J. Environ. Manag.* **2015**, *150*, 92–102. [[CrossRef](#)] [[PubMed](#)]
70. Baumbach, L.; Siegmund, J.F.; Mittermeier, M.; Donner, R.V. Impacts of Temperature Extremes on European Vegetation during the Growing Season. *Biogeosciences* **2017**, *14*, 4891–4903. [[CrossRef](#)]
71. Chapin, F.S.; Starfield, A.M. Time lags and novel ecosystems in response to transient climatic change in arctic Alaska. *Clim. Chang.* **1997**, *35*, 449–461. [[CrossRef](#)]
72. Sukopp, H.; Wurzel, A. The effects of climate change on the vegetation of central European cities. *Arboric. J.* **2000**, *24*, 257–281. [[CrossRef](#)]
73. Musau, J.; Patil, S.; Sheffield, J.; Marshall, M. Spatio-temporal vegetation dynamics and relationship with climate over East Africa. *Hydrol. Earth Syst. Sci.* **2016**. [[CrossRef](#)]

